Available online at www.sciencedirect.com
SCIENCE DIRECT
Thermochimica Acta 437 (2005) 179–189
thermochimica acta
www.elsevier.com/locate/tca

Relation between mobility factor and diffusion factor for thermoset cure

Yan Meng, Sindee L. Simon *

Department of Chemical Engineering, Texas Tech University, Lubbock, TX 79409-3121, USA

Received 16 September 2004; received in revised form 19 May 2005; accepted 21 June 2005
Available online 8 August 2005

Abstract

The temperature-modulated differential scanning calorimetry (TMDSC) responses during cure of both epoxy/aromatic amine and dicyanate ester/polycyanurate systems are modeled using chemical reaction kinetics with diffusion control. Physical aging effects are incorporated into the model using the Tool–Narayanaswamy–Moynihan (TNM) equation. We investigate the assumption that the mobility factor, which may be obtained from experimental temperature-modulated differential scanning calorimetry reversing heat flow data, is related to the diffusion factor for the two systems.

Keywords: Thermoset cure; Modulated DSC; TMDSC; Mobility factor; Diffusion factor; Physical aging

1. Introduction

Although the idea of temperature-modulated differential scanning calorimetry (TMDSC) dates back to as early as 1971 [1], TMDSC was made commercially available only a decade ago [2–4]. Since then, TMDSC has received considerable attention due to its high sensitivity, high resolution, and ability to separate overlapping phenomena [2–6]. A review has been written [7]. The temperature profile of TMDSC generally consists of a periodic temperature modulation superimposed on a constant heating rate. For a sinusoidal modulation, the temperature profile $T(t)$ is given by

$$T(t) = T_0 + mt + A_T \sin(wt) \quad (1)$$

where T_0 is the starting temperature, m is the underlying heating (cooling) rate, t is time, A_T is the amplitude of temperature modulation, and ω is the angular frequency ($=2\pi/t_p$ where t_p is the period of modulation). Thus, the measured heat flow (HF) is a combination of the responses to both the constant heating rate (slow response) and the temperature modulation (fast response). In order to deconvolute the signals, a common analysis method involves separating the response into reversing and nonreversing heat flow components [2–6]. The reversing component has been associated with sensible heat or heat capacity effects, whereas the nonreversing heat flow has been associated with kinetics effects [7]. For thermosetting cure reactions, it is, thus, possible to follow both the heat of chemical reaction and the heat capacity evolution simultaneously [8–19]. However, in order to separate the heat flows, two assumptions have to be made. First, it is assumed that there is a linear relationship between the temperature and the heat flow [20]. Second, the heat capacity contributions are assumed to go only to the first harmonic, whereas the heat of chemical reactions is assumed to go only to higher harmonics [2,7]. These assumptions often do not hold through the melting transition [21–23], through the glass transition region [24–26], and when the nonreversing heating flow is not zero [27]. In addition, another assumption is that the imposed temperature perturbation does not affect the underlying physical and chemical processes; this assumption is generally valid when the amplitude of modulation is small.

The goal of this work is to test the validity of using TMDSC to study thermoset cure kinetics and, more specifically, to test the purported equality of the mobil-

* Corresponding author. Tel.: +1 806 742 1763; fax: +1 806 742 3552.
E-mail address: sindee.simon@ttu.edu (S.L. Simon).

0040-6031/$ – see front matter © 2005 Elsevier B.V. All rights reserved.
doi:10.1016/j.tca.2005.06.032

ity and diffusion factors. To that end, we simulated the TMDSC responses of an epoxy/aromatic amine resin and a bisphenol M dicyanate ester/polycyanurate system, both of whose cure kinetics have been reported [28,29]. The Tool–Narayanaswamy–Moynihan (TNM) model [30–32] was incorporated into our simulations to describe the effects of the vitrification process and associated relaxation on the heat capacity during cure. Before reporting our results, we first review background concerning thermoset cure and the application of TMDSC to study the cure process. We then describe the model used to simulate the TMDSC response, describe and discuss the results, and end with conclusions.

2. Background

The cure process of thermosetting polymers transforms monomers (or prepregs) into a chemically crosslinked polymer network. Both the fractional conversion (α) and the glass transition temperature (T_g) of the reacting system increase as the cure reaction proceeds. In both isothermal cure and ramp cure, if the cure temperature (T_c) reaches the instantaneous glass transition temperature of the reacting system, vitrification, which results in both an increase in the characteristic relaxation time and a decrease in the mobility of the chain segments [33], will occur. In ramp cure, devitrification will occur subsequently when the cure temperature again surpasses the glass transition temperature of the system.

The process of vitrification normally results in a dramatic increase in the characteristic time scale for the movement of chain segments. Rabinowitch [34] proposed that the time scale for reaction is equal to that for the chemically controlled reaction plus that for diffusion. Thus, diffusion control begins to affect the overall cure kinetics when the characteristic time of diffusion is comparable to that of chemical reaction. If the time scales of chemical reaction and diffusion become comparable at the point of vitrification, then vitrification marks the onset of the change of the reaction rate from chemically controlled kinetics to diffusion-controlled kinetics. In actual systems, however, diffusion control may either become dominant when the material is rubbery and T_g is still well below the cure temperature [29] or it may remain weak even after vitrification [8,28].

TMDSC has been used to study the thermoset cure kinetics and its influence on vitrification during cure [8–19]. Van Mele and coworkers have described a mobility factor (MF) [8,9] to describe vitrification and devitrification during cure as a function of conversion (α) and temperature (T):

$$MF(\alpha, T) \equiv \frac{C_p(\alpha, T) - C_{pg}(\alpha, T)}{C_{pl}(\alpha, T) - C_{pg}(\alpha, T)} \quad (2)$$

where C_p is the reversing heat capacity (C_{prev}) defined by

$$C_{prev} = \frac{A_{HF}}{wA_T} \quad (3)$$

and $C_{pg}(\alpha, T)$ and $C_{pl}(\alpha, T)$ are the heat capacities in the glassy state and equilibrium state (liquid or rubbery state), respectively. For most of the cure systems studied [8–11,14,15,17], the mobility factor has been used to approximate the diffusion factor, which is defined as

$$DF(\alpha, T) = \frac{(d\alpha/dt)_{obs}}{(d\alpha/dt)_{chem}} \quad (4)$$

where $(d\alpha/dt)_{chem}$ is the rate of the chemically controlled kinetics, obtained by modeling the reaction in the chemically controlled region, and $(d\alpha/dt)_{obs}$ is the experimentally observed rate of reaction. However, since diffusion control does not necessarily become dominate at the point of vitrification [8,19,28,29], equating the mobility factor to the diffusion factor does not necessarily hold. Van Mele and coworkers are aware of this point since in an organic system they studied [8], in which motions associated with cure were not restricted by vitrification, the two were not equal. Similarly, in a free radical copolymerization of an unsaturated polyester resin and styrene [35], the relationship between diffusion control and vitrification was complicated by the autoacceleration effect and other aspects of free radical polymerization. More recently, Montserrat and Pla [19] found that the mobility and diffusion factors differed in a catalyzed epoxy/anhydride system; they pointed out that a modulation period shorter than 60 s was required in order for diffusion control to take place in the same conversion region as the frequency-dependent glass transition. As indicated in that work [19], the issue of the frequency dependence of the glass transition (frequency-dependent vitrification) [36] is important since it leads to a frequency-dependent mobility factor which makes the relation of the mobility factor to the diffusion-controlled reaction kinetics and to the diffusion factor even more tenuous [37]. Again, Van Mele and coworkers are aware of this issue [13,17], and the frequency-dependent mobility factor has been discussed [38]. However, in spite of these issues, the use of mobility factors to approximate the diffusion factors has been implicitly advocated [9–15,17].

In addition to using the heat capacity obtained in TMDSC to yield information concerning the significance of diffusion control, Van Mele and coworkers also proposed that the point of vitrification (i.e., when $T_g(\omega)$ equals the cure temperature, T_c) is said to occur when the mobility factor equals 0.5 [9–12]. This seems like a reasonable assumption at first glance since the glass transition temperature, which is defined as the midpoint of the heat capacity step change, coincides with the point when the mobility factor, which is actually a normalized heat capacity, equals 0.5. Because the reversing heat capacity in the glass transition region depends on thermal history and the contributions of enthalpy relaxation to the first harmonic [26], vitrification may not occur exactly at a mobility factor of 0.5. However, the errors arising from the assumption that the heat capacity equals the reversing heat flow are small; simulations of various thermal histories show that the midpoint in the step change of the reversing heat capacity is generally found to be within 1 °C of $T_g(\omega)$ [26]. Hence,

the error incurred by assuming that the frequency-dependent vitrification occurs at mobility factor of 0.5 is expected to be small.

3. Modeling the TMDSC response during cure

To model the TMDSC responses during cure, we need models for both the reaction kinetics and the heat capacity since the measured heat flow (HF) of TMDSC contains contributions from both terms:

$$\mathrm{HF} = C_\mathrm{p}\frac{\mathrm{d}T}{\mathrm{d}t} + H_\mathrm{r}\frac{\mathrm{d}\alpha}{\mathrm{d}t} \tag{5}$$

where C_p is the instantaneous heat capacity of the reacting system, $\mathrm{d}T/\mathrm{d}t$ is the rate of temperature change, H_r is the specific heat of chemical reaction, and $\mathrm{d}\alpha/\mathrm{d}t$ is the rate of change of conversion. Below, we first describe models for the reaction kinetics and, subsequently, for the heat capacity.

Models have been developed for the reaction kinetics of the epoxy/aromatic amine system [28] and the dicyanate ester/polycyanurate system [29] studied, and the models very well describe the evolution of conversion and T_g during isothermal cure for both systems for a range of cure temperatures [28,29]. For the two systems, the chemically controlled rate laws are given by Eqs. (6) and (7), respectively:

$$\frac{\mathrm{d}\alpha}{\mathrm{d}t} = k_0(1-\alpha)^2(\alpha + B) \tag{6}$$

$$\frac{\mathrm{d}\alpha}{\mathrm{d}t} = k_1(1-\alpha)^2 + k_2\alpha(1-\alpha)^2 \tag{7}$$

where B is a constant and the rate constant k_i ($i = 0, 1, 2$) follows the Arrhenius law in the chemically controlled regime:

$$k_i = A_i \exp\left(-\frac{E_i}{RT}\right) \tag{8}$$

where A_i is the pre-exponential factor, E_i is the activation energy, R is the universal gas constant, and T is absolute temperature.

A commonly used approach to describe diffusion-controlled kinetics is the Rabinowitch concept [34], which was employed in modeling the epoxy/aromatic amine and dicyanate ester/polycyanurate systems [28,29]. The overall rate constant k is defined by

$$\frac{1}{k_i(\alpha, T)} = \frac{1}{k_{\mathrm{c},i}(T)} + \frac{1}{k_\mathrm{d}(\alpha, T)} \quad (i = 0, 1, 2) \tag{9}$$

where k_d is the diffusion rate constant and k_c is the chemically controlled rate constant in the absence of diffusion given in Eq. (8). The k_d term for the epoxy/aromatic amine system was derived from the modified WLF equation [28] rather than WLF equation in order to expand its range of application to temperatures below $T_\mathrm{g} - C_2$:

$$k_\mathrm{d} = A_\mathrm{d} \exp\left[\frac{C_1(T - T_\mathrm{g})}{C_2 + |T - T_\mathrm{g}|}\right] \tag{10}$$

where A_d and C_1 are adjustable parameters obtained from curve fitting, C_2 has the same values as in WLF equation, i.e., $C_2 = 51.6$ K. On the other hand, the k_d for the dicyanate ester/polycyanurate system was derived from the modified Doolittle free volume equation as shown in Eqs. (11) and (12) [29]:

$$k_\mathrm{d} = A_\mathrm{d} \exp\left(-\frac{E_\mathrm{d}}{RT}\right) \exp\left(-\frac{b}{f}\right) \tag{11}$$

where A_d and b are adjustable parameters, E_d is the diffusion activation energy for diffusion process, and f is the equilibrium free volume, which has to be greater than zero:

$$f = 0.00048(T - T_\mathrm{g}) + 0.025 \tag{12}$$

T_g of the reacting system is a function of fractional chemical conversion (α). For the epoxy/aromatic amine [39] and dicyanate ester/polycyanurate [29] systems, the T_g versus conversion (α) relationships are given by Eqs. (13) and (14), respectively:

$$T_\mathrm{g}(\alpha) = T_{\mathrm{g}0} + \frac{((E_\mathrm{x}/E_\mathrm{m}) - (F_\mathrm{x}/F_\mathrm{m}))\alpha}{1 - (1 - (F_\mathrm{x}/F_\mathrm{m}))\alpha} T_{\mathrm{g}0} \tag{13}$$

$$T_\mathrm{g}(\alpha) = T_{\mathrm{g}0} + \frac{\alpha\lambda(T_{\mathrm{g}\infty} - T_{\mathrm{g}0})}{1 - (1 - \lambda)\alpha} \tag{14}$$

where $T_{\mathrm{g}0}$ and $T_{\mathrm{g}\infty}$ are the glass transition temperatures of the monomer and fully cured system, respectively; $E_\mathrm{x}/E_\mathrm{m}$ is the ratio of lattice energies for the crosslinked polymer to uncrosslinked polymer and $F_\mathrm{x}/F_\mathrm{m}$ is the ratio of segmental motilities for the crosslinked polymer to uncrosslinked polymer, respectively, and λ is fitting constant. Eq. (13) is the empirical DiBenedetto equation [40] and Eq. (14) is the modified form of the DiBenedetto equation derived from entropic considerations [41]. Although T_g is a function of cooling rate and frequency, this equation assumes a one-to-one relationship between fractional chemical conversion (α) and T_g, and the latter of which is measured at a given cooling rate ($q = 10$ K/min in refs. [28,29]).

The heat capacity evolution during the cure reaction depends on the fractional chemical conversion, cure temperature, and relaxation processes related to the kinetics associated with the glass transition. We consider temperature- and conversion-dependent heat capacities where the quantities are taken to be a linear combination of the heat capacities for the monomer ($C_{\mathrm{p}0}$) and for the fully cured system ($C_{\mathrm{p}\infty}$) as has been assumed by other researchers [42–45]:

$$C_\mathrm{pl}(\alpha, T) = (1 - \alpha)C_{\mathrm{pl},0}(T) + \alpha C_{\mathrm{pl},\infty}(T) \tag{15}$$

$$C_\mathrm{pg}(\alpha, T) = (1 - \alpha)C_{\mathrm{pg},0}(T) + \alpha C_{\mathrm{pg},\infty}(T) \tag{16}$$

where $C_{\mathrm{pl},0}(T)$ is the equilibrium heat capacity for the uncured system, $C_{\mathrm{pg},0}(T)$ is the heat capacity in the glassy state for the uncured system, $C_{\mathrm{pl},\infty}(T)$ is the equilibrium heat capacity for the fully cured system, and $C_{\mathrm{pg},\infty}(T)$ is the heat capacity in the glassy state for the fully cured system. All heat capacity

values are assumed to depend linearly on temperature:

$$C_{\mathrm{pl},0}(T) = a_{\mathrm{l}0} + b_{\mathrm{l}0}T \quad (17)$$

$$C_{\mathrm{pl},\infty}(T) = a_{\mathrm{l}\infty} + b_{\mathrm{l}\infty}T \quad (18)$$

$$C_{\mathrm{pg},0}(T) = a_{\mathrm{g}0} + b_{\mathrm{g}0}T \quad (19)$$

$$C_{\mathrm{pg},\infty}(T) = a_{\mathrm{g}\infty} + b_{\mathrm{g}\infty}T \quad (20)$$

where $a_{\mathrm{l}0}, a_{\mathrm{g}0}, a_{\mathrm{l}\infty}, a_{\mathrm{g}\infty}, b_{\mathrm{l}0}, b_{\mathrm{g}0}, b_{\mathrm{l}\infty}, b_{\mathrm{g}\infty}$ are constants. The value of the step change in the heat capacity at the glass transition temperature, $\Delta C_{\mathrm{p}}(\alpha, T_{\mathrm{g}})$ can be obtained from $C_{\mathrm{pl}}(\alpha, T_{\mathrm{g}}) - C_{\mathrm{pg}}(\alpha, T_{\mathrm{g}})$.

In the glass transition region, the changes in heat capacity can be described by the Tool–Narayanaswamy–Moynihan (TNM) model [30–32]. Extensive work has shown that the TNM model quantitatively predicts the phenomena associated with the glass transition (although it cannot do so with one set of parameters over a wide range of experimental variables) [46,47]. In addition, the model reproduces the TMDSC experimental results for the glass transition region [48–50].

In the TNM model, a normalized heat capacity C_{pn} is defined:

$$C_{\mathrm{pn}} \equiv \frac{C_{\mathrm{p}} - C_{\mathrm{pg}}}{C_{\mathrm{pl}} - C_{\mathrm{pg}}} = \frac{\mathrm{d}T_{\mathrm{f}}}{\mathrm{d}T} \quad (21)$$

where T_{f} is the fictive temperature, which can be calculated numerically by

$$T_{\mathrm{f}}(T) = T_i + \int_{T_i}^{T} \mathrm{d}T' \left\{ 1 - \exp\left[-\left(\int_{T'}^{T} \frac{\mathrm{d}T''}{q\tau} \right)^{\beta} \right] \right\} \quad (22)$$

where T_i is the initial temperature in equilibrium state, β is a constant, q is the rate of temperature change, and τ is relaxation time defined as

$$\tau = \tau_0 \exp\left[\frac{x\,\Delta h}{RT} + \frac{(1-x)\Delta h}{RT_{\mathrm{f}}} \right] \quad (23)$$

where τ_0, x and Δh are all constants, and R is the gas constant. The parameters β, x, and Δh are closely related [46,51,52]. The value of τ_0 depends on conversion or $T_{\mathrm{g}}(\alpha)$ since the relaxation time depends on the relative values of T and T_{g}. We assume $\tau = 100$ s when $T = T_{\mathrm{g}} = T_{\mathrm{f}}$; thus, the parameter τ_0 is given by

$$\tau_0(T_{\mathrm{g}}) = exp\left[\ln(100) - \frac{\Delta h}{RT_{\mathrm{g}}} \right] \quad (24)$$

4. Methodology: simulation of TMDSC responses

For the epoxy/aromatic amine and dicyanate ester/polycyanurate systems modeled, both isothermal and ramp cure TMDSC simulations are performed. In all simulations, the modulation amplitude (A_T) is 0.5 K. A modulation period (t_{p}) of 90 s is used in all epoxy/aromatic amine simulations except when the effect of period on the results is explored; in that case, the period ranges from 60 to 1000 s. The heating rates used in ramp cure simulations of the epoxy/aromatic amine system are 0.10 K/min except when the effect of heating rate on results is explored; in that case the heating rate is 0.06 or 0.08 K/min. For simulations of dicyanate ester/polycyanurate system, the period of modulation is 90 s in isothermal cure and 180 s in ramp cure in which the underlying heating rate is 0.008 K/min; a low ramp rate is used for the dicyanate ester/polycyanurate system in order to achieve vitrification during the ramp due to the slow cure kinetics of the system; the longer period for the slow ramp allows the simulation to be performed in a reasonable amount of time (several days). For ramp cures, the simulation begins by cooling at 15 K/min from a reference temperature ($T_i = 0\,^{\circ}$C), at which both materials are in equilibrium, to 25 °C below $T_{\mathrm{g}0}$, and then the ramp cure is initiated. The ramp goes from $T_{\mathrm{g}0} - 25$ to 220 °C, which is well above $T_{\mathrm{g}\infty}$ for both systems modeled. For the isothermal cure of the epoxy/aromatic amine, the isothermal cure temperatures used are from 80 to 140 °C at 20 °C intervals; for the dicyanate ester/polycyanurate systems the isothermal cure temperature used is 150 °C.

Sixty-four data points are taken per period of modulation, and a fast Fourier transform (FFT) is performed from which the amplitude of the first harmonic (A_{HF}) is obtained. The reversing heat flow is calculated from the first harmonic using Eq. (3). At each point, we use sliding transforms to also get the average cure temperature (T_{ave}) and underlying heat flow (also called the total heat flow). The nonreversing heat flow is obtained from the difference between the underlying heat flow and the reversing heat flow.

The parameters used for the simulations of the epoxy/aromatic amine and the dicyanate ester/polycyanurate systems are listed in Tables 1 and 2, respectively. Cure kinetics and reaction parameters for the epoxy/aromatic amine and

Table 1
Material and TMDSC parameters used for the epoxy/aromatic amine system simulations

Parameter	Value or range	Reference
H_{r} (kJ/g)	0.381 (−23.0 kcal/mol epoxy group equivalent)	[53]
A_0 (s^{-1})	1.28×10^5	[28]
E_0 (kcal/mol)	15.23	[28]
B	5.548×10^{-2}	[28]
A_{d} (min^{-1})	30.64	[28]
C_1	42.61	[28]
C_2 (K)	51.6	[28]
$T_{\mathrm{g}0}$ (°C)	−4.9	[28]
$T_{\mathrm{g}\infty}$ (°C)	178	[28]
$E_{\mathrm{x}}/E_{\mathrm{m}}$	0.52	[39]
$F_{\mathrm{x}}/F_{\mathrm{m}}$	0.31	[39]
$C_{\mathrm{pl}}(\alpha, T)$ ($\mathrm{Jg}^{-1}\,\mathrm{K}^{-1}$)	$(1-\alpha)$ (1.58426 + 0.00325861T) + α(1.94462 + 0.00137894T)	[43]
$C_{\mathrm{pg}}(\alpha, T)$ ($\mathrm{Jg}^{-1}\,\mathrm{K}^{-1}$)	$C_{\mathrm{pl}} - [0.55\,(1-\alpha) + 0.19\alpha]$	[54]
A_T (K)	0.5	
t_{p} (s)	60, 90, 120, 600, 1000	

Table 2
Material and TMDSC parameters used for the dicyanate ester/polycyanurate system simulations

Parameter	Value or range	Reference
H_r (kJ/g)	−0.485	[29]
A_1 (s^{-1})	1.83×10^{11}	[29]
E_1 (kJ/mol)	120	[29]
A_2 (s^{-1})	225	[29]
E_2 (kJ/mol)	44	[29]
A_d (min^{-1})	1.0×10^{19}	[29]
E_d (kJ/mol)	140	[29]
b	0.25	[29]
T_{g0} (°C)	−26	[29]
$T_{g\infty}$ (°C)	182	[29]
λ	0.426	[29]
$C_{pl}(\alpha, T)$ ($Jg^{-1}K^{-1}$)	$(1-\alpha)(1.5784+0.0021T)+\alpha(1.8335+0.0012T)$	[45]
$C_{pg}(\alpha, T)$ ($Jg^{-1}K^{-1}$)	$C_{pl}-[0.4(1-\alpha)+0.2\alpha]$	[55]
A_T (K)	0.5	
t_p (s)	90, 180	

the dicyanate ester/polycyanurate systems are obtained from refs. [28,53] and [29], respectively, and the T_g-conversion relationship parameters are from refs. [39] and [29], respectively. The temperature- and conversion-dependent equilibrium heat capacity values (see Eqs. (15–20)) for the epoxy/aromatic amine system are assumed to be the same as those of an epoxy/fiber composite as in ref. [43], and ΔC_p values at zero and full conversion are taken from ref. [54]. For the dicyanate ester/polycyanurate system, the temperature- and conversion-dependent equilibrium heat capacity is assumed to be the same as another bisphenol A dicyanate ester, which has been reported in the literature [45], and ΔC_p values at zero and full conversion are taken from ref. [55].

Three sets of correlated TNM parameters [51] are used in the modeling and are listed in Table 3. In all simulations except otherwise indicated, the $x = 0.4$ set of TNM parameters is used.

In order to check the effectiveness of using TMDSC to obtain the heat capacity, linear simulations are also performed. The linear simulation is run under quasi-isothermal conditions with an amplitude of 0.01 K and a period of 90 s for a given state of the system (α, T_g, T_{ave}) during cure. The simulation consists of applying the TNM model with $T_f = T$ as the initial condition. After several modulation cycles, the fictive temperature and the reversing heat flow reach steady state values giving the frequency-dependent heat capacity, $C_p(\omega)$.

Table 3
Sets of TNM parameters [51] used in simulations

x	$\Delta h/R$ (K^{-1})	β
0.3	120,000	0.53
0.4	80,000	0.62
0.5	70,000	0.75

5. Results and discussion

The simulation of the TMDSC experiment for the isothermal cure of epoxy/aromatic amine system at 140 °C is shown in Fig. 1, where the average cure temperature (T_{ave}), the glass transition temperature (T_g), and the reversing heat capacity (C_{prev}) along with the equilibrium capacity (C_{pl}) and glassy heat capacity (C_{pg}) are plotted as a function of time. At the beginning of the cure, the average cure temperature (T_{ave}) is well above the initial glass transition temperature of the uncured system (T_{g0}) and the reversing heat capacity (C_{prev}) is the equilibrium value (C_{pl}). The T_g of the reacting system increases with time as cure progresses. As T_g approaches and rises above T_{ave}, C_{prev} shows a stepwise decrease from the equilibrium value to the glassy value. As indicated in the figure, the midpoint of the step change in the reversing heat capacity occurs considerably earlier than the point at which $T_g(q = 10\,K/min) = T_{ave}$. This seeming discrepancy occurs because T_g is frequency-dependent (or rate-dependent). The reversing heat capacity is obtained for $t_p = 90$ s, whereas the T_g values plotted in the figure are based on the T_g-conversion relationship (Eq. (13)) for T_g obtained at a cooling rate of 10 K/min [28]. Hence, the T_g values plotted are lower than those that would be obtained at a modulation period of 90 s, and vitrification, as defined by $T_g(q = 10\,K/min) = T_{ave}$, occurs later than the step change in the reversing heat capacity.

For the isothermal cure of the epoxy/aromatic amine system at 140 °C, the expected heat flow for the chemical reaction and the nonreversing heat flow obtained from the simulation shown in Fig. 1 are shown as a function of time in Fig. 2. The inset shows a zoom-in view for the later cure stages. The rate of reaction calculated from the nonreversing

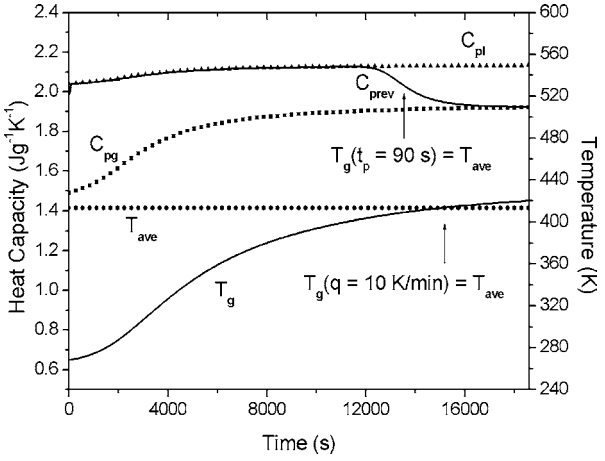

Fig. 1. The glass transition temperature, the average cure temperature, and the reversing, equilibrium, and glassy heat capacities as a function of time for the TMDSC simulation of the epoxy/aromatic amine system cured isothermally at 140 °C with $A_T = 0.5$ and $t_p = 90$ s. The triangles represent the equilibrium heat capacity; the squares represent the glassy heat capacity; the circles represent the average cure temperature; the upper and lower solid line represent the reversing heat capacity and the glass transition temperature, respectively.

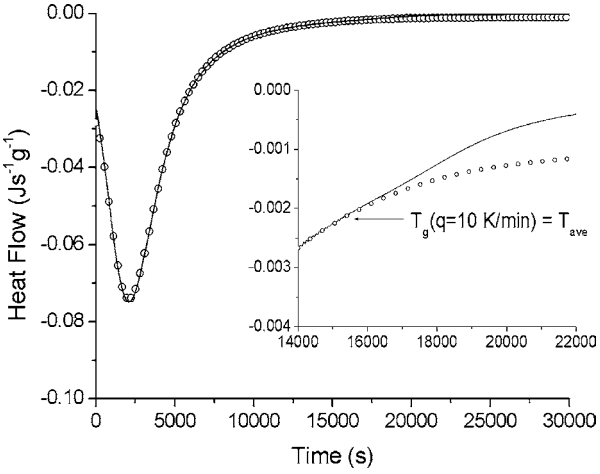

Fig. 2. Expected heat flow from chemical reaction and nonreversing heat flow as a function of time for the TMDSC simulation of the epoxy/aromatic amine system cured isothermally at 140 °C with A_T = 0.5 K and t_p = 90 s. The symbols represent the expected heat flow of reaction from chemical reaction and the solid line represents the nonreversing heat flow. The inset shows the heat flow at the later stages of reaction with vitrification marked.

heat flow agrees with the expected rate of reaction before vitrification, but the two differ after vitrification as can be seen from the inset. The reversing heat capacity, as well as the expected heat capacity from linear simulations, is shown in Fig. 3. No difference was observed between the expected heat capacity and the reversing heat capacity. This is as expected since the system is vitrifying from an equilibrium state to the glass state at constant temperature as the glass transition temperature increases, in an analogy to a cooling run at constant conversion. In such a case, if the change in temperature is slow enough, vitrification will be imposed by the modulation (rather than by the temperature change), and the expected (linear) heat capacity will equal the reversing heat capacity.

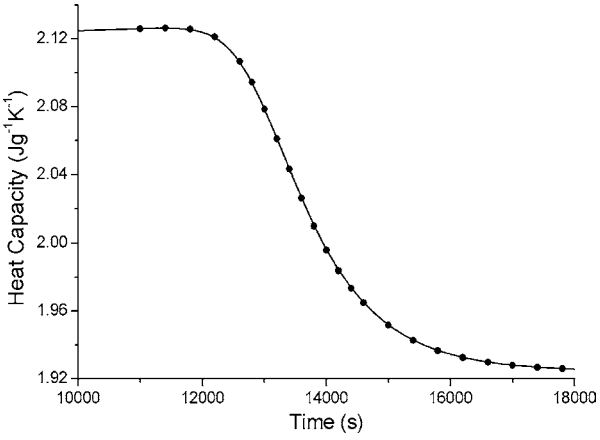

Fig. 3. Expected heat capacity from the linear simulation and reversing heat capacity as a function of time for the TMDSC simulation of the epoxy/aromatic amine system cured isothermally at 140 °C with A_T = 0.5 K and t_p = 90 s. The symbols represent the expected heat capacity from linear simulation and the solid line represents the reversing heat capacity.

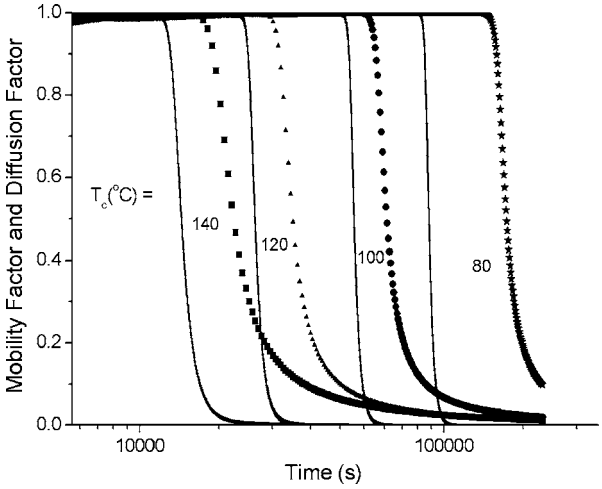

Fig. 4. Mobility factor (MF, in lines) and diffusion factor (DF, in symbols) as a function of logarithmic time for TMDSC simulations of the epoxy/aromatic amine system cured isothermally at 80, 100, 120, and 140 °C (from right to left) with A_T = 0.5 K and t_p = 90 s.

The mobility factor and diffusion factor are compared in Fig. 4 for simulated isothermal cures of the epoxy/aromatic amine system at cure temperatures of 80, 100, 120, and 140 °C. It is obvious that the two do not agree in any of the cases. The drop in the mobility factor occurs at shorter times compared to the drop in the diffusion factor, indicating that diffusion control occurs after $T_g(\omega)$ reaches the isothermal cure temperature. This is the opposite of what was found for an epoxy/anhydride system [19], but it is consistent with the known kinetics [28] of the studied system coupled with the fact that $T_g(\alpha, t_p = 90\,s)$ is higher than $T_g(\alpha, q = 10\,K/min)$. When the results are plotted against conversion rather than time, the mobility factor drops at a conversion 7% lower than the value where the diffusion factor drops for cure at 80 °C; for cure at 140 °C, the difference in the conversions at which the mobility factor and diffusion factor drop decreases to 3%. These differences are significant. However, using a longer modulation period (lower frequency) will move the frequency-dependent mobility factor to longer times (higher conversions) resulting in the better agreement between the mobility factor and the diffusion factor. This effect is discussed in more detail later.

The simulation of the TMDSC response of the epoxy/aromatic amine system in ramp cure at 0.1 K/min is shown in Fig. 5. The average cure temperature (T_{ave}), the glass transition temperature (T_g), and the reversing heat capacity (C_{prev}), along with equilibrium (C_{pl}) and glassy heat capacities (C_{pg}), are plotted as a function of time. As can be seen in Fig. 5, the glass transition temperature of the uncured system (T_{g0}) is higher than the cure temperature at the beginning of the cure and the reversing heat capacity is the glassy value. As the cure temperature increases above T_{g0}, the system undergoes initial devitrification, and the reversing heat capacity shows a stepwise increase to the equilibrium (liquid) heat capacity value. As the cure temperature increases

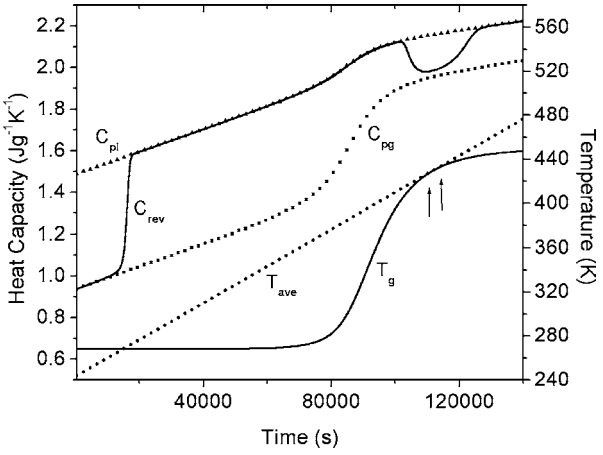

Fig. 5. The glass transition temperature, the average cure temperature, the reversing, equilibrium and glassy heat capacities as a function of time for the TMDSC simulation of the epoxy/aromatic amine system during ramp cure at 0.10 K/min with $A_T = 0.5$ K and $t_p = 90$ s. The triangles represent the liquid heat capacity; the squares represent the glassy heat capacity; the circles represent the average cure temperature; the upper and lower solid line represent the reversing heat capacity and the glass transition temperature, respectively. The two arrows mark the points of vitrification and devitrification as defined by T_g ($q = 10$ K/min) = T_{ave}.

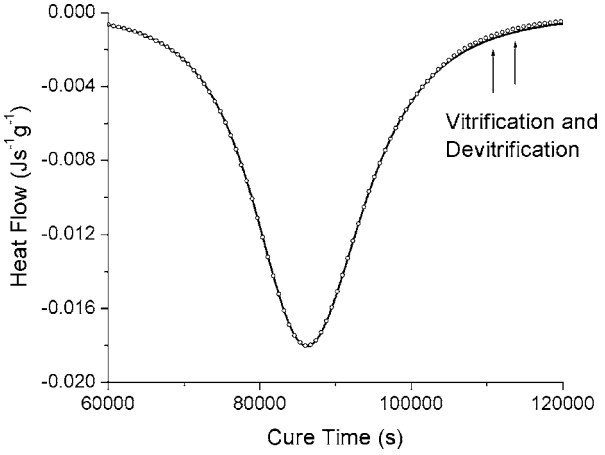

Fig. 6. Expected heat flow and nonreversing heat flow, as a function of time for the TMDSC simulation of the epoxy/aromatic amine system during ramp cure at 0.10 K/min with $A_T = 0.5$ K, $t_p = 90$ s. The open circles represent nonreversing heat flow; the solid line stands for expected heat flow from chemical reaction. The two arrows indicate the points of vitrification and devitrification as defined by T_g ($q = 10$ K/min) = T_{ave}.

further, the chemical reaction begins resulting in an increase both in fractional chemical conversion and in T_g, as well as a slight increase in C_{pl} due to its conversion dependence. As T_g approaches T_{ave}, the reversing heat capacity also decreases towards the glassy value. As the temperature scan continues, the average cure temperature increases further; T_{ave} rises above T_g, which is leveling off due to completion of the reaction, devitrification occurs, and the reversing heat capacity increases back to its equilibrium value. We note that in the ramp cure, as in the isothermal cure, the points of vitrification (and devitrification) as defined by the midpoint in $C_{prev}(T_g(t_p = 90\,s) = T_{ave})$ are not equal to those defined by $T_g(q = 10$ K/min) = T_{ave}; this is as expected due to the rate and frequency dependence of T_g.

The nonreversing heat flow calculated from the TMDSC ramp cure simulation shown in Fig. 5 is compared to the expected heat flow based on the reaction kinetics in Fig. 6. The points of vitrification and devitrification defined by $T_g(q = 10$ K/min) = T_{ave} are denoted by the two arrows. As in the isothermal case (Fig. 2), the expected heat flow agrees well with nonreversing heat flow in regions far from the transition region; however, the two deviate in the vicinity of transition region due to enthalpy relaxation effects that also contribute to the nonreversing heat flow in this region.

The reversing heat capacity for the ramp cure simulation is compared to its expected values obtained from linear simulations shown in Fig. 7. Similar to the heat flow comparison, the expected heat capacity and the reversing heat capacity deviate only in the vicinity of the transition region (the belly of the curve). This suggests that contributions from physical relaxation or chemical reaction may contribute to the first harmonic and lead to an error in the reversing heat capacity, consistent with the results of previous work [26].

The mobility factor (MF) calculated from the reversing heat capacity (see Eq. (2)) shown in Fig. 5 is plotted in Fig. 8 along with the diffusion factors (DF), which is defined as the ratio of the rate of reaction to the rate if the reaction were chemically controlled (see Eq. (4)), both of which are obtained from the model. In addition, we plot the diffusion factor obtained from the nonreversing heat flow (DF_{non}), which is defined as the ratio of rate of reaction obtained from the nonreversing heat flow (assumed to be due only to chemical reaction) to the rate if the reaction were chemically

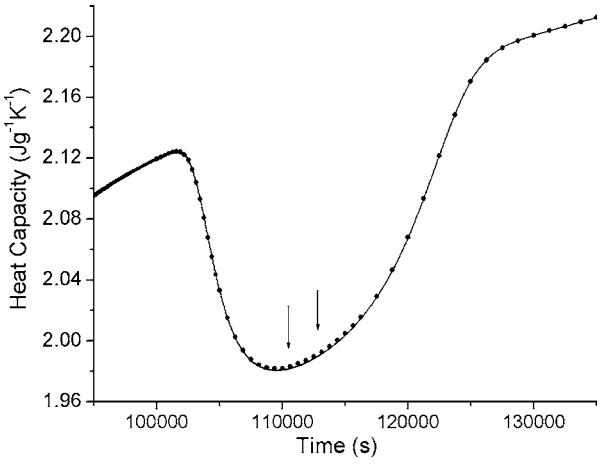

Fig. 7. The expected heat capacity and reversing heat capacity as a function of time for the TMDSC simulation of the epoxy/aromatic amine system during ramp cure at 0.10 K/min with $A_T = 0.5$ K and $t_p = 90$ s. The circles represent expected reversing heat capacity value from linear simulation; the solid line represents reversing heat capacity from the simulation. The two arrows indicate the points of vitrification and devitrification as defined by T_g ($q = 10$ K/min) = T_{ave}.

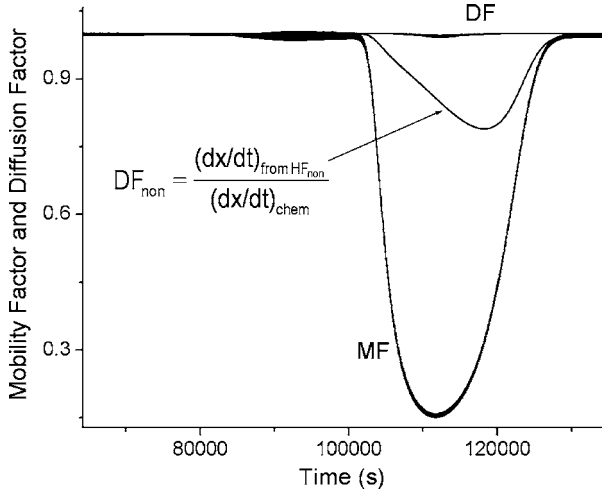

Fig. 8. The mobility factor and diffusion factor as a function of time for the epoxy/aromatic amine system during ramp cure at 0.10 K/min with $A_T = 0.5$ K and $t_p = 90$ s. Also shown is the diffusion factor calculated from the nonreversing heat flow.

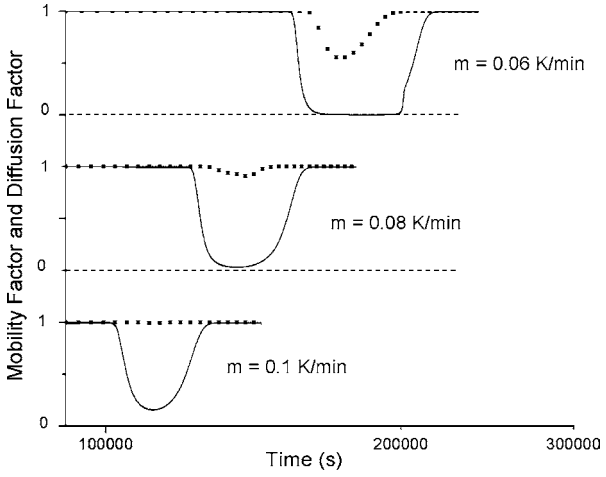

Fig. 9. Mobility factor (MF, in lines) and diffusion factor (DF, in symbols) as a function of logarithmic cure time for the TMDSC simulation of the epoxy/aromatic amine system cured at ramp rates of 0.06, 0.08, and 0.10 K/min with $A_T = 0.5$ K and $t_p = 90$ s.

controlled. The diffusion factor is close to unity during the whole cure process because of the weak diffusion effect specific for this cure system and the small overshoot of T_g over T_{ave}. It is clear that the mobility factor does not equal the diffusion factor for this system. On the other hand, the diffusion factor obtained from the nonreversing heat flow (DF_{non}) and the mobility factor (MF) follow similar trends: both decrease in the vicinity of vitrification and increase back in the vicinity of devitrification. However, DF_{non} is influenced by the effect of enthalpy relaxation associated with vitrification, which results in a difference between the expected and observed nonreversing heat flow. The influence of enthalpy relaxation on the mobility and diffusion factors has been neglected in experimental studies. We note that, experimentally, it is impossible to differentiate diffusion control from enthalpy relaxation effects in the nonreversing heat flow without more information. The comparisons of mobility and diffusion factors on a logarithmic time scale are shown in Fig. 9 for the heating rate of 0.1 K/min and for two slower heating rates, 0.08 and 0.06 K/min. In all cases, the results are similar to those shown in Fig. 8 with significant discrepancy between the mobility factor and diffusion factor.

In the isothermal and ramp cure simulation results described in Figs. 1–9, we assume that the heat capacity was temperature- and conversion-dependent. Simulations were also performed assuming constant values for C_{pg} and C_{pl}, with no effects on the results, i.e., (i) the reversing and nonreversing heat flows well represent $C_p(\omega)$ and the heat of reaction, respectively, with only small discrepancies due primarily to physical aging effects, and (ii) the mobility factor does not equal the diffusion factor.

As mentioned previously, the reversing heat capacity varies with the period of modulation, so simulations of the ramp cure at 0.1 K/min were performed using other periods of modulation. The evolution of the reversing heat capacities is shown in Fig. 10 for $t_p = 90$, 600, 1000 s. The dynamic glass transition temperature decreases as the period of modulation increases, resulting in devitrification occurring at earlier times in the ramp cure and vitrification occurring at later times. The mobility factor mirrors the changes in C_{prev} as is shown in Fig. 11. The period of modulation obviously has a large effect on the value of the mobility factor. As the period of modulation increases, the extent of vitrification obtained from the frequency-dependent reversing heat capacity becomes weaker and the difference between the mobility factor and the diffusion factor decreases.

In addition, we also examined the effect of the changing the TNM parameters, using parameter sets shown in Table 3 for $x = 0.3$ and 0.5. The mobility factor as a function of time for a ramp cure for the three different TNM parameters sets investigated is shown in Fig. 12. The TNM parameters affect

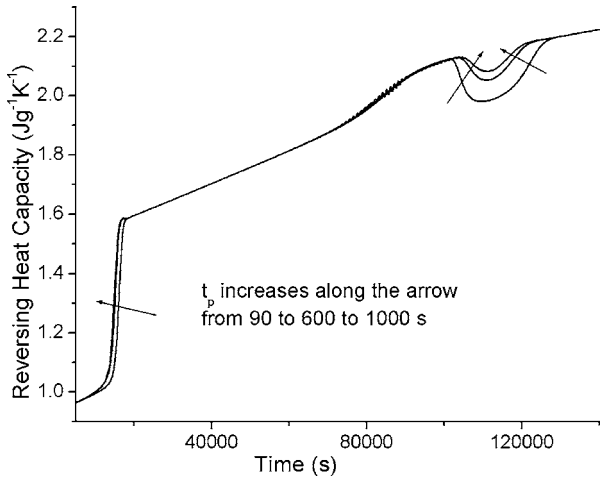

Fig. 10. The reversing heat capacity as a function of time for epoxy/aromatic amine system at 0.10 K/min obtained for ramp cure simulations using various modulation periods with $A_T = 0.5$ K.

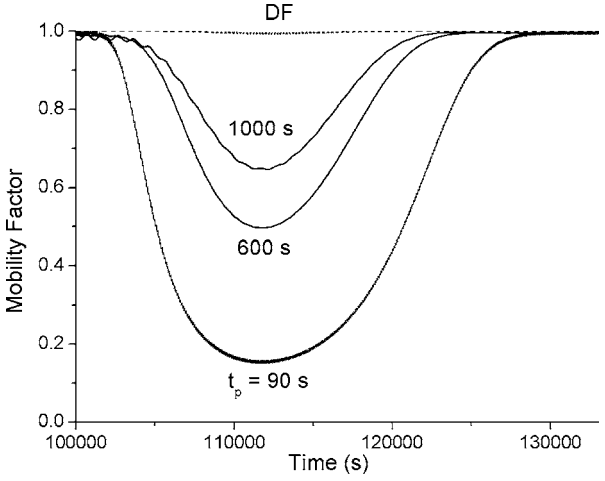

Fig. 11. The mobility factor as a function of time for epoxy/aromatic amine system during ramp cure at 0.10 K/min for various modulation periods with A_T = 0.5 K. The dashed line represents the diffusion factor.

the mobility factor; however, the effect is not as great as the effect of changing the period of modulation.

In addition to the TMDSC cure simulations described for the epoxy/aromatic amine system, we also simulated the cure of a dicyanate ester/polycyanurate resin in which the kinetic model and parameters differ significantly from the epoxy/aromatic amine system. The mobility factor and the diffusion factor for the dicyanate ester/polycyanurate system are plotted as a function of time in Fig. 13 for an isothermal cure simulation at 150 °C. The evolution of T_g is also plotted, as is the average cure temperature (T_{ave}). For the dicyanate ester/polycyanurate system, the diffusion effect is particularly strong well before vitrification (as defined by $T_g(q = 10\,K/min) = T_{ave}$), presumably because the reaction involves three reacting groups coming together rather than two; thus, unlike for the epoxy/aromatic amine system shown

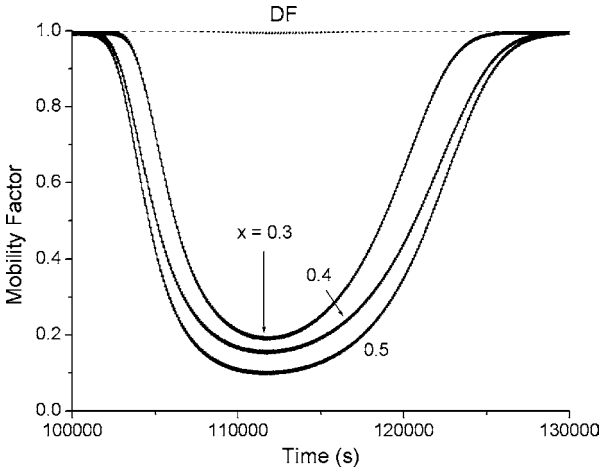

Fig. 12. The mobility factor as a function of time for epoxy/aromatic amine system during ramp cure at 0.10 K/min for various TNM parameter sets and with A_T = 0.5 K and t_p = 90 s. The value of x is given; the values of the other parameters can be obtained from Table 3. The dashed line represents the diffusion factor.

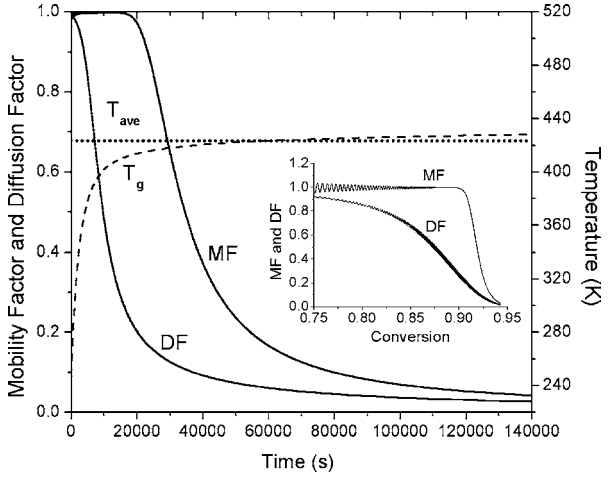

Fig. 13. The mobility factor (MF) and diffusion factor (DF) as a function of cure time for the dicyanate ester/polycyanurate system cured at 150 °C with A_T = 0.5 K and t_p = 90 s. The circles represent the average cure temperature, and the dashed line represents the glass transition temperature of the reacting system. The inset shows the mobility factor and diffusion factor as a function of conversion.

in Fig. 4, the drop in the diffusion factor occurs well ahead of the mobility factor. The inset shows the dependence of the mobility and diffusion factors as a function of conversion; the difference in the conversion at a given value ranges from greater than 20% at the point at which the diffusion factor drops, to approximately 10% for a value of the mobility and diffusion factor of 0.8, to less than 2% for values less than 0.2. Similarly for the simulations of a ramp cure of the dicyanate ester/polycyanurate system, the mobility factor and diffusion factor do not coincide, as shown in Fig. 14. After the initial devitrification, the mobility factor remains very close to one and only drops in the vicinity of vitrification, whereas the value of the diffusion factor remains below 0.1 even after the initial devitrification because of the

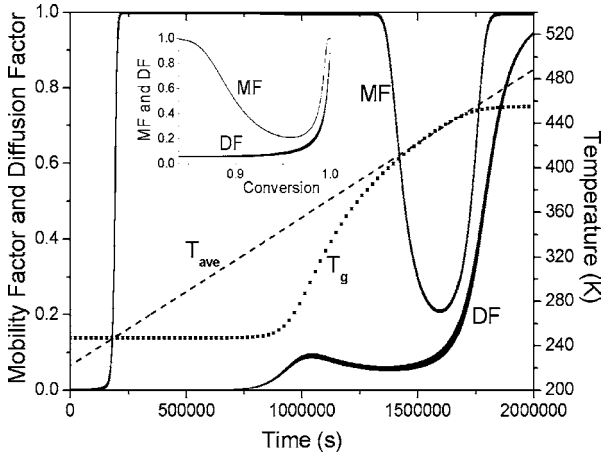

Fig. 14. The mobility factor and diffusion as a function of cure time for the dicyanate ester/polycyanurate system in ramp cure at 0.008 K/min with A_T = 0.5 K and t_p = 180 s. In addition, T_g (squares) and T_{ave} (dashed lines) are shown. The inset shows the mobility factor and diffusion factor as a function of conversion at the later stages of the ramp cure.

strong temperature-dependent diffusion effects in the model (see Eq. (11)). At later times, in the vitrification region, the mobility factor decreases and then subsequently increases on devitrification, whereas the diffusion factor increases to unity only well after the final devitrification when the reaction is essentially completed ($\alpha > 0.99$). When the results are plotted against conversion, the differences between the mobility factor and diffusion factor are large at low conversions (due to the fact that the diffusion factor is very low, whereas the mobility factor is high). However, at the very late stage of cure (when the reaction is essentially completed), the two are nearly the same, being offset from one another by only 1% conversion, as shown in the inset in Fig. 14. As already mentioned, a slow heating rate of 0.008 K/min was used in the ramp cure simulation for the dicyanate ester/polycyanurate in order that vitrification occurs during the ramp cure due to the slow cure kinetics of the system.

6. Conclusions

The TMDSC responses of both an epoxy/aromatic amine and a dicyanate ester/polycyanurate cure system are modeled for both isothermal and ramp cures, and the mobility factor obtained from the reversing heat capacity is calculated and compared with the diffusion factor. The effects of ramp rate, isothermal cure temperature, input heat capacities, modulation periods, and TNM parameters are discussed. The results show that the mobility factor is not equal to the diffusion factor for either system modeled for a variety of modulation and cure conditions. However, the difference in the conversion at a given value of the mobility factor and the diffusion factor can range from very large to as small as 1%, the latter of which is well within the experimental error of conversion. Hence, in some systems under certain cure conditions, the mobility factor may be used to approximate the diffusion factor. Deciding when and where this approximation can be made without considerable modeling and experimentation is, however, problematic. The mismatch between the mobility factor and the diffusion factor is perhaps not surprising because the transition from chemically controlled kinetics to diffusion-controlled kinetics need not occur exactly at vitrification. In addition, since T_g is frequency (or cooling rate)-dependent, vitrification as defined by $T_g(\omega) = T_{ave}$ is also frequency-dependent underscoring its lack of significance for predicting the onset of diffusion control. The effect of enthalpy relaxation can be important and can influence the calculated diffusion factor.

Acknowledgement

The authors gratefully acknowledge NSF DMR 0308762 for financial support.

References

[1] H. Gobrecht, K. Hamann, G. Willers, J. Phys. E. 4 (1971) 21–23.
[2] M. Reading, Trends Polym. Sci. 1 (8) (1993) 248–253.
[3] G.S. Gill, S.R. Sauerbrunn, M. Reading, J. Therm. Anal. 40 (1993) 931–939.
[4] M. Reading, D. Elliott, V.L. Hill, J. Therm. Anal. 40 (1993) 949–955.
[5] U. Jorimann, G. Widmann, R. Riesen, J. Therm. Anal. Calorim 56 (1998) 639–648.
[6] E. Verdonck, K. Schaap, L.C. Thomas, Int. J. Pharm. 192 (1999) 3–20.
[7] S.L. Simon, Thermochim. Acta 374 (2001) 55–71.
[8] G. Van Assche, A. Van Hemelrijck, H. Rahier, B. Van Mele, Thermochim. Acta 268 (1995) 121–142.
[9] G. Van Assche, A. Van Hemelrijck, H. Rahier, B. Van Mele, Thermochim. Acta 286 (1996) 209–224.
[10] G. Van Assche, A. Van Hemelrijck, H. Rahier, B. Van Mele, Thermochim. Acta 304/305 (1997) 317–334.
[11] B. Van Mele, G. Van Assche, A. Van Hemelrijck, J. Reinf. Plast. Comp. 18 (1999) 885–894.
[12] S. Montserrat, I. Cima, Thermochim. Acta 330 (1999) 189–200.
[13] G. Van Assche, B. Van Mele, Y. Saruyama, Thermochim. Acta 377 (2001) 125–130.
[14] S. Montserrat, J.G. Martin, J. Appl. Polym. Sci. 85 (2002) 1263–1276.
[15] S. Montserrat, F. Roman, P. Colomer, Polymer 44 (2003) 101–114.
[16] S. Swier, G. Van Assche, B. Van Mele, J. Appl. Polym. Sci. 91 (2004) 2798–2813.
[17] S. Swier, G. Van Assche, B. Van Mele, J. Appl. Polym. Sci. 91 (2004) 2814–2833.
[18] J.E.K. Schawe, Thermochim. Acta 391 (2002) 279–295.
[19] S. Montserrat, X. Pla, Polym. Int. 53 (2002) 326–331.
[20] J.E.K. Schawe, Thermochim. Acta 260 (1995) 1–16.
[21] G.W.H. Hohne, Thermochim. Acta 330 (1999) 93–99.
[22] B. Wunderlich, A. Boller, I. Okazaki, K. Ishikiriyama, W. Chen, M. Pyda, J. Pak, I. Moon, R. Androsch, Thermochim. Acta 330 (1999) 21–38.
[23] R. Scherrenberg, V. Mathot, A. Van Hemelrijck, Thermochim. Acta 330 (1999) 3–19.
[24] J.E.K. Schawe, Thermochim. Acta 271 (1996) 127–140.
[25] J.E.K. Schawe, S. Theobald, J. Non-Cryst. Solids 235–237 (1998) 496–503.
[26] S.L. Simon, G.B. McKenna, Thermochim. Acta 348 (2000) 77–89.
[27] S.X. Xu, Y. Li, Y.P. Feng, Thermochim. Acta 343 (2000) 81–88.
[28] G. Wisanrakkit, J.K. Gillham, J. Coat. Tech. 62 (1990) 35–50.
[29] S.L. Simon, J.K. Gillham, J. Appl. Polym. Sci. 47 (1993) 461–485.
[30] A.Q. Tool, J. Am. Ceram. Soc. 29 (1946) 240–253.
[31] O.S. Narayanaswamy, J. Am. Ceram. Soc. 54 (1971) 491–497.
[32] C.T. Moynihan, P.B. Macedo, C.T. Montrose, P.K. Gupta, M.A. DeBolt, J.F. Dill, B.E. Dom, P.W. Drake, A.J. Easteal, P.B. Elterman, R.P. Moeller, H. Sasabe, J.A. Wilder, Ann. N.Y. Acad. Sci. 279 (1976) 15–35.
[33] J.K. Gillham, Polym. Eng. Sci 26 (20) (1986) 1429–1433.
[34] E. Rabinowitch, Trans. Faraday Soc. 33 (1937) 1225–1233.
[35] G. Van Assche, E. Verdonck, B. Van Mele, Polymer 42 (2001) 2959–2968.
[36] N.O. Birge, S.R. Nagel, Phys. Rev. Lett. 54 (1985) 2674–2677.
[37] J.E.K. Schawe, Thermochim. Acta 391 (2002) 279–295.
[38] G. Van Assche, S. Swier, B. Van Mele, Thermochim. Acta 388 (2002) 327–341.
[39] X. Wang, J.K. Gillham, J. Appl. Polym. Sci. 47 (1993) 447–460.
[40] L.E. Nielsen, J. Macromol. Sci. Rev. Macromol. Chem. C3 (1969) 69–103.
[41] A.T. DiBenedetto, J. Polym. Sci., Part B 25 (1987) 1949–1969.
[42] G. Van Der Plaats, Thermochim. Acta 72 (1984) 77–82.

[43] J.L. Baillbul, D. Delaunary, Y. Jarny, J. Reinf. Plast. Comp. 15 (1996) 479–496.
[44] V.L. Zvetkov, Polymer 42 (2001) 6687–6697.
[45] J. Dupuy, E. Leroy, A. Maazouz, J.P. Pascault, M. Raynaud, E. Bournez, Thermochim. Acta 388 (2002) 313–325.
[46] I.M. Hodge, J. Non-Crystalline Solids 169 (1994) 211–266.
[47] G.B. McKenna, Comprehensive polymer science, in: C. Booth, C. Price (Eds.), Polymer Properties, vol. 12, Pergamon, Oxford, 1999, pp. 311–362.
[48] J.M. Hutchinson, S. Montserrat, Thermochim. Acta 304/305 (1997) 257–265.
[49] S.L. Simon, G.B. McKenna, Thermochim. Acta 348 (2000) 77–89.
[50] S. Weyer, M. Merzlyakov, C. Schick, Thermochim. Acta 377 (2001) 85–96.
[51] I.M. Hodge, J. Res. Natl. Inst. Stand. Technol. 102 (1997) 195–205.
[52] I.M. Hodge, Macromolecules 15 (1982) 762–770.
[53] S.L. Simon, J.K. Gillham, J. Appl. Polym. Sci. 46 (1992) 1245–1270.
[54] G. Wisanrakkit, J.K. Gillham, unpublished work.
[55] S.L. Simon, J.K. Gillham, unpublished work.